Renewable and Sustainable Energy Reviews 32 (2014) 206–221

Contents lists available at ScienceDirect

Renewable and Sustainable Energy Reviews

journal homepage: www.elsevier.com/locate/rser

A review of wind loads on heliostats and trough collectors

Honghang Sun [a], Bo Gong [b,*], Qiang Yao [a]

[a] Department of Thermal Engineering, Tsinghua University, Beijing 100084, China
[b] The Key Laboratory of Solar Thermal Energy and Photovoltaic System, Institute of Electrical Engineering, Chinese Academy of Sciences, No. 6 Beiertiao, Zhongguancun, Beijing 100190, China

ARTICLE INFO

Article history:
Received 7 June 2013
Received in revised form
20 November 2013
Accepted 4 January 2014
Available online 31 January 2014

Keywords:
Heliostat
Trough collector
Wind load

ABSTRACT

This article reviews existing papers and presents considerations about wind loads on heliostats and trough collectors. Research efforts all over the world have focused, for decades, on the evaluation and reduction of wind loads on heliostats and trough collectors. However, the subject continues to be a live issue, since scientists are attempting to find a low-cost and highly accurate solution. In this paper, we will review the effects of wind loads on heliostats and trough collectors, considering wind flow characteristics, turbulence intensity and the Reynolds number, the aspect ratio, porosity and mirror gap, wind loads on isolated collectors and on collector fields, and the effects of wind on beam quality. This review is expected to be of use to researchers and engineers involved in the analysis and design of heliostats and trough collectors.

Contents

* Corresponding author. Tel.: +86 10 82547035; fax: +86 10 62587646.
E-mail address: gongbo1979@163.com (B. Gong).

1364-0321/$ - see front matter
http://dx.doi.org/10.1016/j.rser.2014.01.032

Nomenclature

Abbreviations

CSP	concentrating solar power
LEC	levelized electricity cost
ABL	atmospheric boundary layer
PSD	power spectral density
Re	Reynolds number
BCS	beam characterization system

Symbols

A	the solid area of the heliostat
A_B	the solid blockage area of upwind heliostat and fences
A_F	the ground area occupied be the upwind blockage units
B	the empirical constant and its magnitude based on the observed wind profiles
$C_{Pi}(t)$	the time history of net pressure coefficient difference of the tap i
C_{Fx}	horizontal force coefficient
C_{Fz}	vertical force coefficient
C_{My}	base overturning moment coefficient
C_{MHy}	hinge moment coefficient
C_{Mz}	azimuth moment coefficient
$C_{pi,\ max}$	peak positive pressure coefficient
$C_{pi,\ min}$	peak negative pressure coefficient
$C_{pi,mean}$	mean pressure coefficient
$C_{pi,rms}$	fluctuating pressure coefficient
f	the Coriolis parameter
F_x	horizontal force
F_z	vertical force
g	peak value factor
G_B	generalized blockage area
h	the chord length of the heliostat
H	the height of the center of the heliostat area from ground
I_u	longitudinal turbulence intensity
I_v	lateral turbulence intensity
k	Von Karman′s constant
L_u^x	longitudinal turbulence integral length scale
M_y	base overturning moment
M_{Hy}	hinge moment
M_z	azimuth moment
n	frequency
$P_i^f(t)$	measured front surface pressures at the tap i
$P_i^b(t)$	measured back surface pressures at the tap i
Q	dynamic pressure of the mean approaching wind
$S_u(n)$	PSD of longitudinal fluctuating wind speed
$U(10)$	mean wind speed at 10 m height from the ground
$U(z_{ref})$	mean wind speed at the reference height z_{ref}
$U(z)$	mean wind speed at height z
U_0^*	surface friction velocity
z	the height from ground
z_d	the aero-plane displacement
z_0	the surface roughness length
z_G	the gradient height
z_{ref}	the reference height from ground
α_0	the ground roughness exponent
α	the pitch angle
β	the yaw angle
σ_u	standard deviation of longitudinal fluctuating wind speed
σ_v	standard deviation of lateral fluctuating wind speed
ρ	the air density

1. Introduction

Over the last few years, we have witnessed wild fluctuations and a clear upward trend of fossil fuel prices. Price uncertainty is a serious economic risk factor for new power plants [1]. Renewable energies have huge potential to achieve the goal of reducing fossil fuel consumption, thus stabilizing costs and minimizing adverse environmental effects [2].

There are three main renewable technologies with different performance characteristics, namely wind power technology, photovoltaic technology and concentrating solar power (CSP) technology. CSP systems use concentrated solar radiation to generate high temperatures, which are later employed to drive a conventional power cycle and produce electricity. The main categories of CSP are solar power tower, parabolic trough, dish system and Fresnel reflectors [3]. Heliostats and trough collectors constitute the main investment costs of tower and trough systems respectively [4]. This will be discussed in detail in this paper.

The main features of CSP technology rather than other renewable technologies are its thermal energy storage capacity, balancing power, backup capacity and flexible design. The thermal energy storage capacity allows for additional flexibility in the power supply and increases the full load equivalent operating hours. The balancing capacity means that a higher share of variable renewable power (wind power and photovoltaic power) will be enabled by the complementary implementation of balancing renewable power (concentrating solar power). Backup capacity refers to the fact that fossil fuel backup can be used to drive the turbine of CSP systems as a complementary source of energy [5,6]. The solar collector field size and the capacity of the thermal energy storage can be optimized to achieve the flexible design goal. The worldwide CSP industry has grown 40% since 2005 and is expected to reach installed capacity of 4.5 GW in 2013 [6,7]. Therefore, substantial scale effects, technology improvements and investment cost reduction are expected for the CSP industry.

Undoubtedly, the current levelized electricity costs (LEC) of wind power and photovoltaic systems are lower than the LECs of CSP, which is CSP′s main disadvantage when competing with other technologies [5,8]. The estimated competitiveness of the various renewable power systems for the year 2020 is analyzed in Table 1 [5,9]. The increments of investment costs of renewable technologies and fossil fuel prices have been taken from available literature. Table 1 shows that CSP investment costs will be significantly reduced and will become competitive with wind power and photovoltaic systems by 2020. Fig. 1 shows the current costs of tower and trough systems in the CSP industry to give an idea of their development potential for the future [4,10,11]. The cost of heliostats is presently estimated in the range of 150 and

Table 1
Overview on specific investment of different renewable power supplies for the 2020 scenario [5,9].

Specific cost (investment)	Unit	Value
CSP Power Block	€/kW	1078
Photovoltaic	€/kWp	940
Wind power	€/kW	1208
Gas turbine	€/kW	400

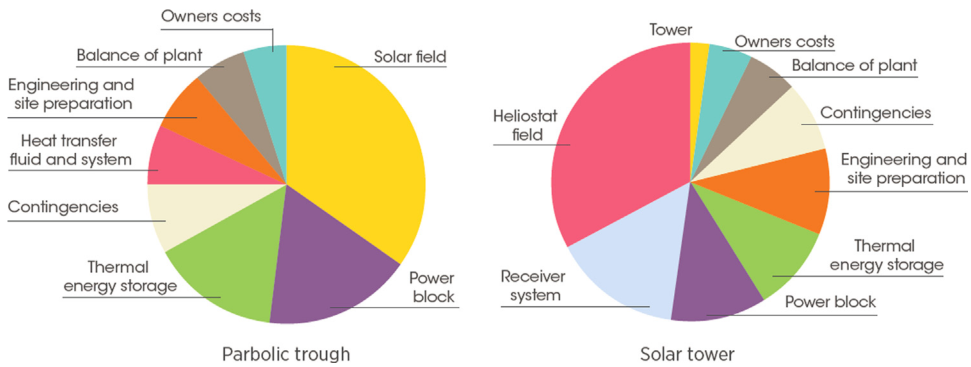


Fig. 1. The current installed cost for 100 MW trough and tower CSP plants in South Africa [4,10,11].

200 USD/m^2 and the cost of targets generally varies between 75 and 120 USD/m^2 [6]. This indicates that costs may lower even more in the future.

Most of the money invested in CSP systems goes to the solar collector fields. Thus, costs may be reduced by determining the wind loads on collectors. These collectors, which must be highly accurate, are located at open or suburban areas and are sensitive to gusts. Therefore, the stationary and dynamic effects of wind will be the major design parameter for the structure and the drive systems [12].

Measurements of wind loads on ground-based solar collectors have been obtained in wind tunnel tests. The study of wind loads on solar collectors began in the late 1970s under the sponsorship of Sandia National Laboratories, Colorado State University, Martin Marietta Corporation and McDonnell Douglas Astronautics Company [13–16]. These studies measured the mean wind loads on heliostats and trough collectors. The importance of dynamic wind loads effects on collectors was reviewed by Peterka et al. [17–20]. The first design of the experiment had several problems because only the effects of static wind in the collector were considered. Therefore, dynamic effects due to fluctuating and peak wind loads had to be analyzed to correct these problems [20]. Tests that consider fluctuating wind loads were developed in the early 1990s [20]. However, some issues remain unresolved: the study of wind pressure distribution, wind characteristics around the collector field, the effects of turbulence on wind loads on collectors, the effects of aspect ratio, porosity and mirror gap on wind loads, among others. Since the beginning of 2000, experts have been conducting studies to find answers to these questions; the solutions can have a significant impact on the problem of wind loads on solar collectors.

Wind loads are a decisive aspect of the design of solar collectors and, therefore, they should be accurately understood. While commendable efforts are being made to determine wind loads on collectors using computers, taking measurements on physical models and prototypes is still a more reliable method [21,22]. Having sensitive and accurate transducers and a system with appropriate frequency response is the basic requirement [21,22]. To test models in wind tunnels, experts build a model of the structure scaling down its geometrical characteristics, reproduce the boundary layer flow, choose the number of pressure ports and their location, and choose a reference pressure [21]. Although there has been some progress on wind tunnel testing of solar collectors, there are still many critical phenomena which can only be investigated through prototype measurements. The data obtained from prototype measurements can be used to verify the reliability of wind tunnel test techniques and to refine the numerical models for structure analysis [22].

This paper includes a review of the existing information on the subject. Some specific aspects of wind loads on heliostats and trough collectors will be discussed in detail.

2. Wind characteristics

Field measurements of wind characteristics in the atmospheric boundary layer (ABL) are very useful to further understand wind climates and boundary layer wind structure. Meanwhile, the conclusions of wind characteristics are also important, since they help scientists to adjust Codes of Practice to wind-resistant designs of structures and to apply the codes to wind tunnel modeling and numerical simulation. The height of solar collectors is usually around 15 m; this enables experts to analyze wind characteristics around heliostats and trough collectors. The wind flow at 15 m is highly turbulent and the wind loads acting on collectors are significantly influenced by the characteristics of the approaching turbulent flow [20,22]. Therefore, the information about wind characteristics currently available is reviewed here to better understand wind flows around solar collectors.

2.1. Wind speed profile models

Information on vertical distribution of wind speed in the ABL over various types of terrains is essential, since this is an important aspect of wind characteristics. Several theoretical and empirical models, such as power law, log law and Deaves–Harris model, have been used to describe the vertical distribution of mean wind speed in the ABL [23–26].

The wind speed profile with power law is the profile most widely used in the world as the load code because of its simplicity [23]. The power law profile would not describe well the vertical distribution of wind speed at lower heights. Mostly, it seems to be applicable to heights between 30 m and 300 m [27]. It can be expressed as follows:

$$\frac{U(z)}{U(z_{ref})} = \left(\frac{z}{z_{ref}}\right)^{\alpha_0} \tag{1}$$

where $U(z)$ is the mean wind speed at height z, $U(z_{ref})$ is the mean wind speed at the reference height z_{ref}, and α_0 is the ground roughness exponent.

Some micrometeorological researchers thought the log law profile met the lowest boundary conditions below 100 m [24,27–29]. However, this profile is invalid at a higher point (above 200 m) [27,30]. The log law profile can be written as follows [23,24]:

$$U(z) = \left(\frac{U_0^*}{k}\right)\ln\left(\frac{z-z_d}{z_0}\right) \tag{2}$$

where U_0^* is the surface friction velocity, k is Von Karman's constant, z_0 is surface roughness length and z_d is the aero-plane displacement.

The Deaves–Harris profile model is thought to be applicable to the entire ABL [25,26]. It is expressed as follows:

$$\frac{U(z)}{U_0^*}=\frac{1}{k}\left\{\ln\left(\frac{z}{z_0}\right)+5.75\frac{z}{h}-1.88\left(\frac{z}{h}\right)^2-1.33\left(\frac{z}{h}\right)^3+0.25\left(\frac{z}{h}\right)^4\right\};\ h=\frac{U_0^*}{Bf} \quad (3)$$

where B is an empirical constant and its magnitude is based on the observed wind profiles and f is Coriolis parameter.

2.2. Wind speed requirements

Second-generation heliostats were developed between 1977 and 1981 [31]. In order to prepare detailed plans and cost estimates for the mechanical and optical performances, these heliostats were tested at the Central Receiver Test Facility in Albuquerque, New Mexico [32]. An important technical result of the test was the definition of heliostat design specifications, shown in Table 2 [32,33]. These include critical beam quality, wind load deflection and survival wind speed corresponding to the optical and mechanical performances that have always been recommended for heliostat designs. The most important consequence of these specifications was the modification of commercial heliostat design to incorporate specific performance requirements.

Taking into account safety and economy considerations, wind speed requirements for solar collectors were identified combining the information obtained from wind tunnel tests and the guidance contained in the Building Design Code of USA, shown in Table 3 [34]. This Table lists the wind speeds to be considered when designing the collector. It should be noted that the various CSP technologies have different wind speed requirements. In the case of heliostats, the ability to endure high winds is an important issue. However, wind-induced deflections are also a major concern, since heliostats must be accurately pointed to their targets for proper operation. In trough collectors, pointing accuracy during operation is less important than in heliostats, because of the shorter focal length [34].

Table 2
s-Generation heliostat design requirements [32,33].

Category	Requirements
Operational modes	Normal modes (track, standby, wire walk, stow) Track in up to 35 mph wind Slew in 50 mph wind Resolve tracking singularity in 15 min Reposition in 15 min Emergency defocus in 3 min Electrical transients (operate through a 3 cycle dropout)
Optical performance	Beam quality (theoretical beam shape plus 1.4 mrad fringe, 32–122 F) Wind load deflection (3.6 mrad RMS maximum reflector surface deflection in 27 mph wind, discounting foundation) Foundation deflection (0.45 mrad maximum set after survival, 1.5 mrad maximum twist or tilt in 27 mph wind)
Survival	90 mph wind, heliostat stowed 50 mph wind, heliostat in any orientation Temperature, −20 to 122 F Hail, 3/4 in. at 65 ft/s, any orientation; 1 in. at 75 ft/s, heliostat stowed Cold water shock
30 Year life	Life of all components must be cost effective for 30 years Mirror and drive mechanism are critical components

2.3. Turbulence characteristics

Solar collectors are in the field with highly turbulent and wind-induced dynamic effects are significantly influenced by the characteristics of the approaching turbulent flow [20,35,36]. The parameters of turbulent flow for collectors are turbulence intensity and power spectral density (PSD). Turbulence intensity is the ratio of the standard deviation of fluctuating wind speed with respect to the mean speed. Turbulence intensity expresses the intensity of fluctuating speed and can be written as follows:

$$I_i=\frac{\sigma_i}{U(z)} \quad (i=u,v) \quad (4)$$

where I_u and I_v are longitudinal and lateral turbulence intensity respectively. σ_u and σ_v are standard deviation of longitudinal and lateral fluctuating wind speed respectively.

In the Building Codes of Japan [37], the longitudinal turbulence intensity can be empirically expressed as follows:

$$I_u=0.1(z_G/z)^{\alpha_0+0.05} \quad (5)$$

where z_G is the gradient height.

The energy distribution of fluctuating wind speed can be expressed in the form of PSD. The empirical expressions of PSD are widely used by Davenport [38] and Karman [39].

$$\frac{nS_u(n)}{U_0^{*2}}=\frac{4x^2}{[1+x^2]^{4/3}} \quad x=\frac{1200n}{U(10)} \quad (6)$$

where n is the frequency, $U(10)$ is the mean wind speed at 10 m from the ground, U_0^* is the friction velocity, and $S_u(n)$ is the PSD of longitudinal fluctuating wind speed.

$$\frac{nS_u(n)}{\sigma_u^2}=\frac{4L_u^x n/U(z)}{[1+70.7(L_u^x n/U(z))^2]^{5/6}} \quad (7)$$

where L_u^x is the longitudinal turbulence integral length scale.

With respect to wind flow simulation in wind tunnels, Banks and Pfahl [40,41] stated that, peak wind loads on solar collectors from wind tunnel data were higher the numbers obtained from field measurements, if the simulated turbulence intensities in wind tunnels are equal to the data of field measurements. The premise of the wind flow simulation refers to collector models with scales of 1:10 and 1:40 in wind tunnels. No conclusions have been reached for collector models with smaller scales. Therefore, the similarity of energy spectral density of approaching wind flow from empirical observations and wind tunnel data would lead to more realistic results of peak wind loads on collectors for model scales between 1:10 and 1:40 [41].

Table 3
Critical design wind speed being recommended for solar collector design [34].

Collector technology	Heliostat	Trough collector	Dish collector
Maximum survival wind speed (mph)	90 At stow position	80 At stow position	100 At stow position
Design wind speed for normal operation (mph)	27	25	36
Maximum operational wind speed (mph)	50	50	36
Stated or implied mean recurrence internal (year)	100 (extreme)	ground mounted: 25, roof mounted: 50 (extreme)	100 (extreme)

3. Effects of turbulence intensity and Reynolds number on wind loads

In the field of wind engineering, turbulence intensity is defined to analyze turbulence characteristics of approaching wind flow. Turbulence intensity represents the force of fluctuating wind speed. It varies with different ground roughness exponents and it decreases as height from the ground increases. Therefore, high turbulence occurs near the ground, below 10 m of height, which is basically within the range of height of solar collectors and its magnitude is around 20% [20,22]. In wind tunnels, the variation of their simulated turbulence intensity influences fluctuating wind pressures on collector models significantly. This conclusion needs to be verified in order to determine wind loads on collectors accurately.

Based on the similitude principle of the Reynolds number (Re), unrealistic high wind speed needs to be achieved in the boundary layer wind tunnel tests in order to have similar wind flows in the wind tunnel and in the actual field. The simulated conditions are hard to recreate in these wind tunnel tests [20,21]. Fortunately, current research results indicate that wind load coefficients of sharp-edged bodies do not depend on Re. In contrast, in structures with round edges, wind load coefficients will significantly vary beyond a certain critical Re [42,43]. The circular torque tube of heliostats and the parabolic mirror edges of trough collectors might be a source of such Re-dependent wind load coefficients.

3.1. Effects of turbulence intensity on wind loads of heliostats

In the ABL, turbulence intensity decreases as height increases. The turbulence intensity profile basically agrees with the power-law profile [37]. In an open field environment, the value of turbulence intensity near the ground is between 15% and 20% [20,22]. When experimentation on this subject began, heliostat models were analyzed in a wind tunnel test having a near-zero intensity [44,45]. Later, wind flow with turbulence intensities of 1.2%, 12%, 14% and 18% were used to measure wind load coefficients of heliostats in wind tunnels [13,17,18]. Fig. 2 shows the comparative results of six experiments with different turbulence intensities simulated in wind tunnels [20]. The conclusion is that wind load coefficients of heliostats increase dramatically for turbulence intensities above 10%. Atmospheric turbulence should be considered in wind tunnel tests so as to determine accurate load coefficients of heliostats [20].

3.2. Effects of turbulence intensity on wind loads of trough collector

The variation of turbulence intensities influences the values of wind load coefficients of heliostats. The occurrence of a similar phenomenon in trough collectors needed to be investigated. With turbulence intensities of 8%, 15% and 21%, a series of wind tunnel tests on an isolated trough collector were conducted to examine and identify the turbulence effects [46]. The values of mean horizontal force coefficients vary slightly as turbulence intensities increase. The effect of turbulence was found to be insignificant for trough collectors when the turbulent approaching flow was simulated properly in the wind tunnel [46].

3.3. Effects of the Reynolds number on wind loads of heliostats

Wind tunnel measurements of heliostats were taken assuming heliostats were sharp-edged bodies. The effects of Re were not considered in these measurements [20,21]. The validity of the hypothesis needs to be verified and the reason is that the circular torque tube of heliostats might cause load coefficients to be dependent on Re. Six-force components of heliostat models at

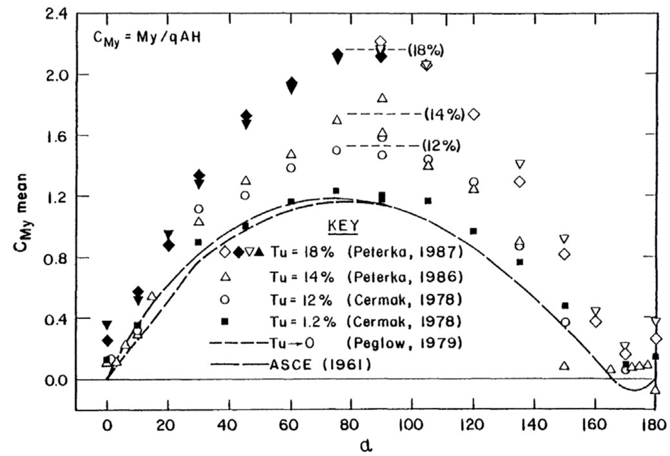


Fig. 2. The variation of mean base overturning moment coefficients with elevation angle and turbulence intensity [20].

stow position were tested to verify the effects of the Re, with a variation of Re from 0.2×10^6 to 1.7×10^6 [43]. No design-relevant Re dependency of the wind load coefficients of heliostats at stow position was measured. Thus, it is valid to determine the wind load coefficients of heliostat at conventional boundary layer wind tunnels at low Re [43].

3.4. Effects of the Reynolds number on wind loads of trough collectors

The parabolic mirror edge might be a source of Re-dependent wind load coefficients of trough collectors. A series of wind tunnel tests were conducted to test the sensitivity of wind load coefficients of trough collectors to Re [46]. Mean horizontal and vertical forces were measured and analyzed, with a Re variation from 2.5×10^4 to 5.5×10^4, in order to verify the effects of the Re on the load coefficients of trough collectors. Results show that the load coefficients do not depend on the Re for the range tested [46].

4. Wind loads on isolated solar collectors

Solar collectors are either tracking the sun (normal operation) or at stow position (at night or during cloudy or very windy periods). Wind loads on the collectors during normal operation are a concern because deformation of mirror surfaces can cause a loss of efficiency. During strong wind, where the structure strength might be a concern, the collectors are typically rotated to stow position so as to limit wind loads and to prevent mirror surfaces from being damaged.

In fields, solar collectors are grouped to form an array made up of individual units. The wind loads on a collector should be analyzed considering the interference of neighboring collectors. However, wind loads on an isolated collector can be regarded as a baseline for characterizing mechanical and optical performances.

4.1. Wind force components on isolated heliostats

Heliostats are located at open fields and they are sensitive to gusts, but nevertheless, their performance needs to be highly accurate. Therefore, wind loads should be an important factor in design. Until now, wind load estimates for heliostats mainly depended on wind tunnel tests. Wind tunnel tests can generate detailed and additional data that is not available in field measurements.

Peterka and Derickson [20] introduced a design method by defining wind loads on isolated heliostats. A force balance was used to measure force components of the heliostat in their experiment and the corresponding wind force coefficients are listed in Table 4 for comparison purposes [20,21,47]. The coordinate system of force components of heliostats is defined in Fig. 3. The following are the expressions of force components [20]:

$$F_x = C_{Fx} Q A \quad (8)$$

$$F_z = C_{Fz} Q A \quad (9)$$

$$M_y = C_{My} Q A H \quad (10)$$

$$M_{Hy} = C_{MHy} Q A h \quad (11)$$

$$M_z = C_{Mz} Q A h \quad (12)$$

where C_{Fx}, C_{Fz}, C_{My}, C_{MHy} and C_{Mz} are the coefficients of horizontal force, vertical force, base overturning moment, hinge moment and azimuth moment, respectively. Q is the dynamic pressure of the mean approaching wind, A is the solid area of the heliostat, h is chord length of the heliostat and H is the height in the center of the heliostat area.

The wind tunnel model adopted had an ideal shape and did not include supporting trusses [20]. Then, Pfahl et al. [47] and Wu et al. [21] conducted wind tunnel tests to determine the force component coefficients of heliostats considering the effects of supporting trusses. The force component coefficients they obtained are also listed in Table 4, showing the maximum mean and peak values for comparison purposes.

Compared to fluctuating wind forces, the determination of mean force components should be a simple exercise. Measurements in wind tunnels have led to the information available today about force component coefficients, on which the heliostat designs are based. However, it is worth noting that the values of mean force component coefficients vary, even for the most straightforward cases, as shown in Table 4. There are probably two reasons that account for the differences amongst the results of wind tunnel studies. The first is that experimental models vary in aspects such as the geometrical details and model material. As regards geometrical details, different supporting trusses might significantly modify the wind flow around the collectors and wind loads on the collectors. The material used in the balanced models must be sufficiently rigid and lightweight in order to measure dynamic wind loading accurately, but this is unknown for the three tests. The second category can be described as “wide gap problem”, which would increase wind loads on collectors [47].

4.2. Wind pressure distribution on isolated heliostats

In addition to force components, pressure distribution and fluctuating pressure characteristics are essential factors in

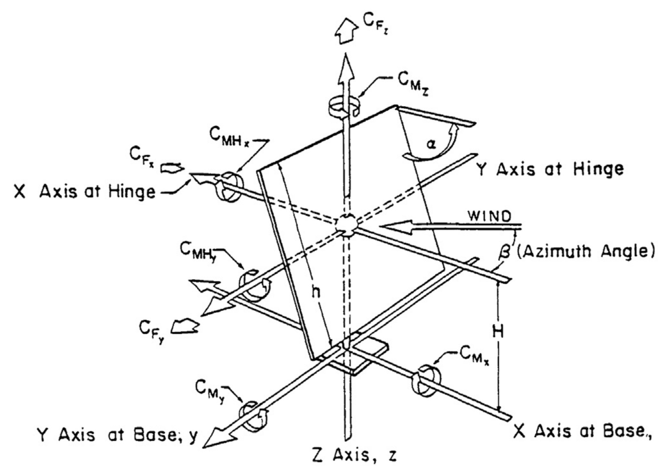


Fig. 3. The coordinate system of force components of heliostat [20].

Table 4
(a) Comparison of maximum mean wind load coefficients [20,21,47].

	Peterka	Gong	Phahl	Peterka	Gong	Phahl
	$Max\lvert C_{Fx}\rvert$			$Max\lvert C_{Fz}\rvert$		
β	0	0	0	0	0	0
α	90	90	90	30	30	30
Value	2.0	1.4	1.5	1.35	0.9	1.0
	$Max\lvert C_{My}\rvert$			$Max\lvert C_{Mz}\rvert$		
β	0	0	0	65	60	60
α	90	90	90	90	90	90
Value	2.0	1.6	1.5	0.25	0.15	0.18
	$Max\lvert C_{MHy}\rvert$					
β	0	150	0			
α	30	30	30			
Value	0.25	0.26	0.18			

(b) Comparison of maximum peak wind load coefficients [20,21,47].

	Peterka	Gong	Phahl	Peterka	Gong	Phahl
	$Max\lvert C_{Fx}\rvert$			$Max\lvert C_{Fz}\rvert$		
β	0	0	0	0	0	0
α	90	90	90	30	30	30
Value	4.0	None	3.3	2.8	None	2.1
	$Max\lvert C_{My}\rvert$			$Max\lvert C_{Mz}\rvert$		
β	0	0	0	65	60	60
α	90	90	90	90	90	90
Value	4.5	None	3.2	0.7	None	0.5
	$Max\lvert C_{MHy}\rvert$					
β	0	150	0			
α	30	30	30			
Value	0.6	None	0.55			

heliostat design that should be taken into account when analyzing dynamic effects. The pressure coefficients can be defined as follows:

$$C_{Pi}(t) = \frac{P_i^f(t) - P_i^b(t)}{(1/2)\rho U(z_{ref})^2} \quad (13)$$

where $C_{Pi}(t)$ is the net pressure coefficient difference of the tap i between the front and back surfaces, ρ is air density and $P_i^f(t)$ and $P_i^b(t)$ are front and back surface pressures at the tap i respectively.

According to the analysis of $C_{Pi}(t)$, mean wind pressure coefficients $C_{pi,mean}$ and fluctuating wind pressure coefficients $C_{pi,rms}$, peak positive and peak negative pressure coefficients of measuring points are as follows:

$$C_{pi,\ max} = C_{pi,mean} + gC_{pi,rms} \quad (14)$$

$$C_{pi,\ min} = C_{pi,mean} - gC_{pi,rms} \quad (15)$$

where $C_{pi,\ max}$ and $C_{pi,\ min}$ are peak positive and peak negative pressure coefficients respectively. $C_{pi,mean}$ and $C_{pi,rms}$ are mean and fluctuating pressure coefficients respectively and g is peak value factor.

Two hundred and eighty eight pressure taps were arranged on the front and back sides of the heliostat model to measure and analyze fluctuating pressure characteristics [48]. Wind pressure fields with and without Gaussian characteristics were analyzed and presented for most load configurations. Most importantly, peak wind pressure distributions were obtained for typical load configurations, as shown in Fig. 4 [48]. The distributions can be used directly to calculate wind-induced responses by finite element analysis. And they can indicate the mechanism of the wind flow behavior around the heliostat.

The yaw angle β defined the azimuth of the heliostat and the pitch angle α defined the tilt with respect to the vertical plane. At $\beta = 90^0$ or $\alpha = 0^0$, wind flow is parallel to the mirror surface and high suctions occur at windward mirror edges due to flow separation at the edges. From $\beta = 0^0$ to $\beta = 90^0$, the pressure distributions are mostly influenced by approaching flow turbulence. From $\beta = 90^0$ to $\beta = 180^0$, the incoming wind acts on the back surface of the heliostat directly and wind pressure values are relatively small, influenced by the shielding effects of supporting components and torque tube [48,49].

4.3. Wind force components on isolated trough collectors

In designing and manufacturing trough collectors, it is essential to have a precise knowledge of wind loads on collectors. This is because the wind loads are critical parameters in selecting an optimum structure design which influences the manufacturing costs significantly.

The isolated trough collector model was tested with and without a torque tube in wind tunnel tests [46]. The coordinate system of force components of trough collectors is defined in Fig. 5 [46]. Fig. 6 shows the horizontal and vertical force coefficients for the isolated collector as a function of the pitch angle obtained by the balance measurement [46]. Besides wind tunnel tests, field measurement is also an effective method for obtaining wind load data about structures. The combination of wind tunnel tests and field measurements can further verify the reliability of measured wind load data. The field measurements of wind loads on prototypical trough collectors were conducted in suburban areas of Beijing City, and the measured wind speed was between 8 m/s and 10 m/s during experimental procedure [22]. Fig. 7 shows the horizontal and vertical force coefficients of the prototypical collector as a function of the pitch angle obtained by integrating the distribution of the measured local pressures [22].

Compared with Figs. 6 and 7, the variation trends of horizontal and vertical force coefficients are consistent. The values of force coefficients are a little different from each other. In wind tunnel tests, the maximum horizontal and vertical forces would be observed at pitch angles of 25° and 60° [46]. In field measurements, the idem horizontal and vertical forces would occur at pitch angles of 45° and 60° [22]. As shown in Fig. 6, the torque tube can affect the load fluctuations considerably. The effect of the torque tube is more obvious for the vertical force than for the horizontal force [46].

4.4. Wind pressure distribution on isolated trough collectors

The data about wind pressure distribution has been obtained through wind tunnel tests conducted on isolated trough collectors [46]. The pressure distributions obtained from field measurements are given in Fig. 8 on the vertical plane by unfolding curved surfaces, illustrating the evident regulations of wind flow around isolated trough collector under wind action [22]. Fig. 8 shows that the magnitudes of mean net pressure coefficients in the areas around the torque tube of the collector vary greatly, indicating that the cylindrical torque tube wake generates separation, when the flow passes through it. It can been seen in Fig. 8 that high pressures are typically concentrated around the edges of the collector because of flow separation or vortex formation from the corner where most wind damage, such as breakage of the mirror panels, is expected to occur [22].

5. Wind loads on solar collectors in fields

Most efforts to determine wind loads and pressures on solar collectors have concentrated on improving the database and its accuracy to account for collector variables and flow variables, dealing with a single collector. Moreover, the need to understand and quantify wind loading effects on fields of solar collectors has emerged as an important study issue. Understanding this is important for the cost-effective design of both conventional collectors and innovative low-cost concepts. This study was undertaken mainly to find methods for reducing wind loads within a collector field to values well below those acting on an isolated collector. The methods for reduction depend on perimeter wind fences, in-field wind fences and field density.

5.1. Wind loads on heliostats in fields

In megawatt solar tower power stations, hundreds of heliostats are laid out in rows and columns. Wind loads on these heliostats are influenced greatly by the field density and wind fences. For example, due to the protection of perimeter wind fences, a major reduction of wind loads on exterior heliostats was observed in wind tunnel tests [17,18].

A number of wind tunnel tests were conducted by Peterka and Cermak from 1978 to 1988 [13,14,16–19]. To reproduce a heliostat field, more than 200 non-instrumented collector models surrounding the instrumented ones were laid out. All these collector models can rotate with elevation and azimuth angles. To further understand the wind load reduction effects of a heliostat field, several aspects on wind load reduction were analyzed in these tests [13,14,16–19].

In Phase 1, scientists conducted tests to observe the effects of external and internal wind fences on wind loads of heliostats at different locations within an array of collectors. The experimental results showed that external wind fences provide significant reduction in wind loads on exterior heliostats and properly designed wind fences surrounding the field can reduce wind loads

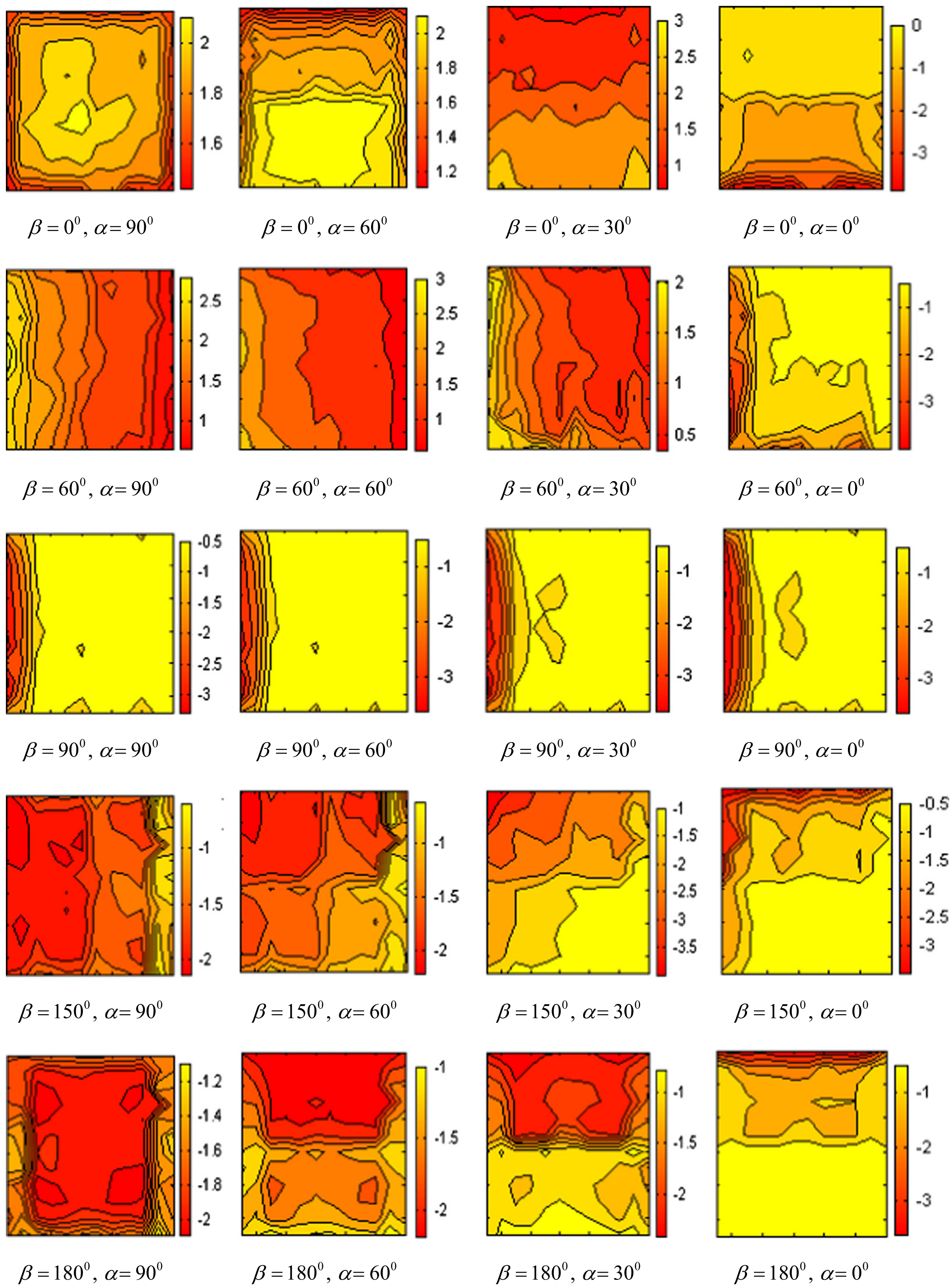


Fig. 4. Peak wind pressure coefficient contours of heliostat [48].

on exterior heliostats to 30%. The increase of internal fences is equivalent to the increase of upwind blockage areas and fosters the steady decrease of the wind loads of interior heliostats. In addition, porosity in the internal fences is also effective for wind load reduction [17,18].

Phase 2 of the tests investigated the effects of field density on wind loads on exterior and interior heliostats. First, wind loads on interior heliostats are substantially lower than those on exterior ones. The former can be as low as 30% of the latter in many cases. Second, the relatively low density of the heliostat field prevents the large wind loading reduction that was observed in the denser field [17,18].

Phase 3 summarizes wind load reduction effects attributable to wind fences and field density. The regulation of wind load reduction is shown in Fig. 9, which illustrates the effects of wind fences and field density [17,18]. The upwind fences and heliostats of different field densities were regarded as solid blockage areas in the approaching wind direction. The generalized blockage area can be defined as follows:

$$G_B = A_B / A_F \quad (16)$$

where A_B is solid blockage area of upwind heliostat and fences, A_F is ground area occupied by the upwind blockage units included in the calculation of A_B, and G_B is the generalized blockage area.

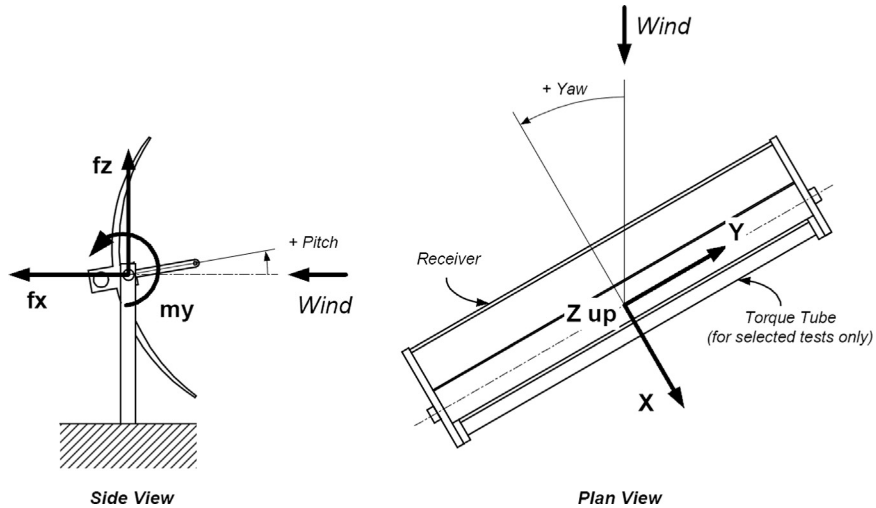


Fig. 5. The coordinate system of force components of trough collector [46].

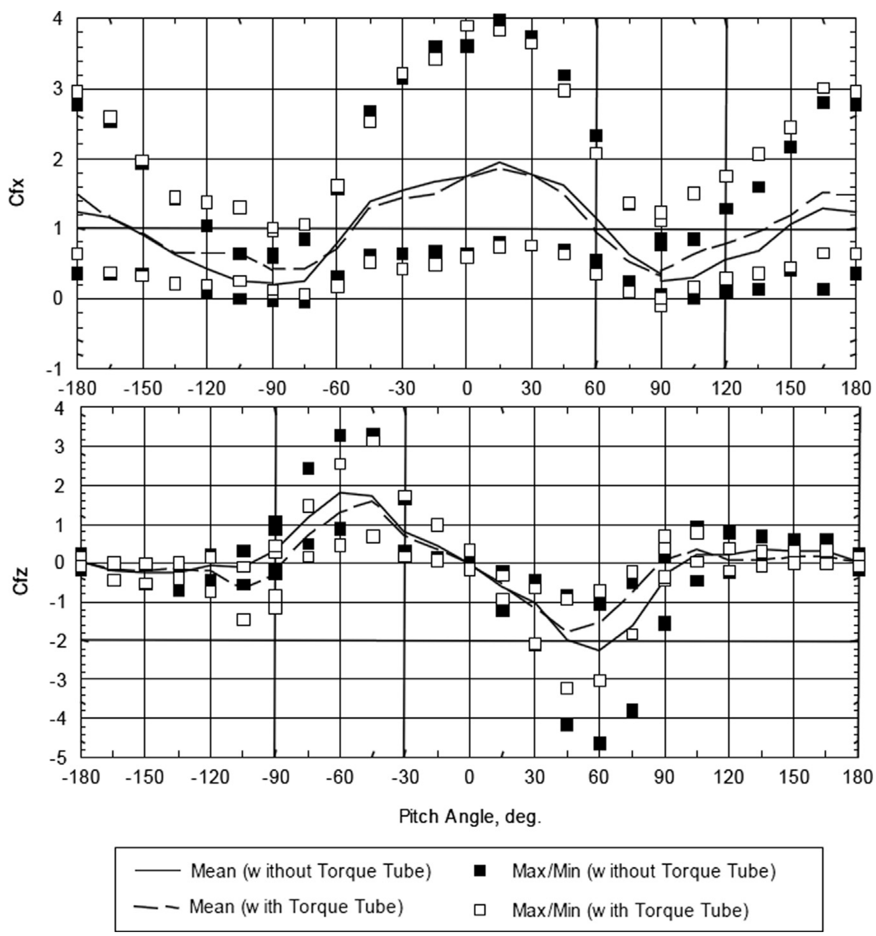


Fig. 6. The horizontal and vertical force coefficients of isolated trough collector tested in wind tunnel [46].

According to Fig. 9, force component coefficients are equal to or lower than the values of the fitting curve from the expression $\exp(-5.56G_B)$. This means that the expression can be regarded as a design guide for calculating wind load coefficients of interior heliostats, which describes the quantity of upwind solid blockage area required to achieve the desired level of load reduction. The increases of wind fences and field density are effective measures to increase blockage areas, in order to achieve the goal reducing wind loads on all the heliostats in a field [17,18].

The reduction of wind loads on heliostats at stow position is also an important issue to be solved so as to improve the design of heliostats. Under strong wind action, the heliostats are usually at stow position, with mirror panels parallel to the approaching wind. The load configuration, whether or not wind loads on

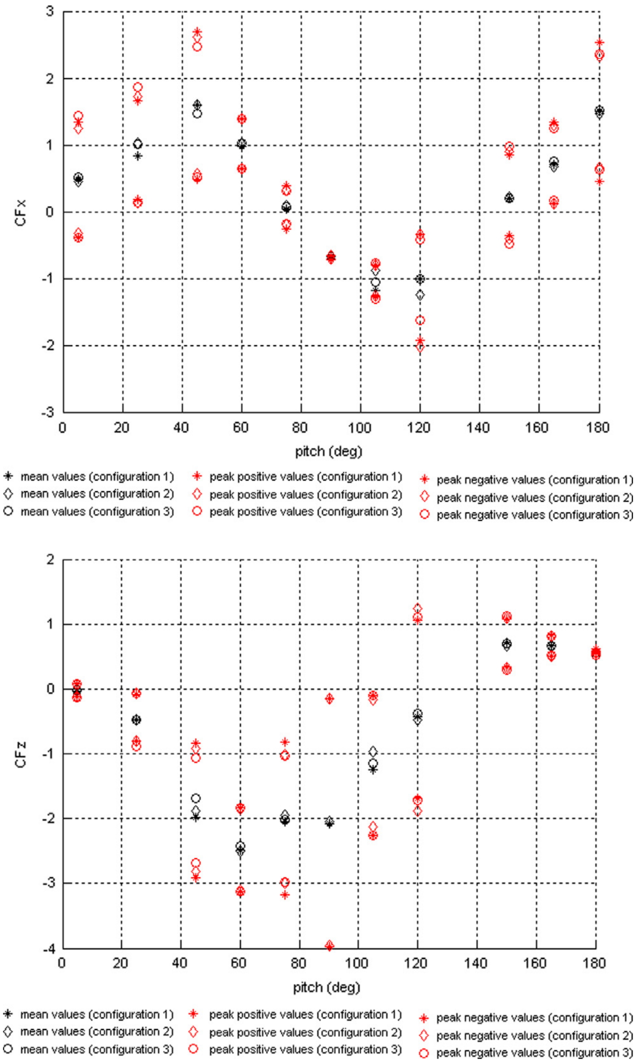


Fig. 7. (a) The horizontal force coefficients of isolated trough collector tested in collector field [22] and (b) The vertical force coefficients of isolated trough collector tested in collector field [22].

interior heliostats are also influenced by wind fences and field density, needs to be tested and analyzed.

Experiments to reduce wind loads on heliostats at stow position were performed in wind tunnel [41]. The regions of low (10–20%), medium (20–40%) and high (> 40%) field density were selected and arranged in the wind tunnel, so as to reproduce the field density effects. Table 5 presents an overview of the main results of reduction of wind loads on heliostats at critical operational and stowed modes [41]. Table 5 shows that force components of interior heliostats will be mostly reduced by the shielding effects of upwind heliostats. In contrast, vertical forces of interior heliostats at stow position will increase, possibly, due to flow separation and vortex shedding effects induced by upwind heliostats. It can also be indicated that high density is more effective for wind load reduction of interior heliostats at stow position [41].

5.2. Wind loads on trough collectors in fields

Trough collectors are laid out in rows in a field with row spacing. All trough collectors rotate around the pitch axis at the same time. Wind loads on the collectors will be influenced by surrounding collectors and wind fences. Until now, a number of wind tunnel tests have been conducted to understand the wind load reduction effects due to the shielding of surrounding collectors and external wind fences [46,50–52].

Conclusions can be summarized as follows [46,50–52]. First, due to shielding effects, downwind trough collectors show large wind load reductions. This conclusion also applies to other types of solar collectors. Second, with appropriate wind protection devices, such as wind fences, wind loads on exterior and interior trough collectors will decrease dramatically. In some cases, the maximum wind loads can be reduced more than 70% for the operation range. Third, gap spacing between trough collectors in a row will not create a significant variation of wind loads on collectors. Row spacing in a field has a minor influence on the wind loads on collectors.

For convenience of wind load design, the entire trough collector field could be divided into three different wind loading zones, including the inner field, the transient field and the edged field. The areas of the inner, transient and edged fields occupy about 95%, 2.5% and 2.5% of the total field, respectively. Corresponding wind loads are applied on trough collectors located at three different wind loading zones [50].

For the purpose of extending design wind load data as a function of position, wind loads reductions in interior trough collectors were examined in wind tunnel tests [46]. The important conclusion is that mean wind loads on trough collectors decrease continually from first to fifth row in the approaching wind direction. At the fifth row, mean wind loads reach their minimum values, regardless of the pitch angle. From the fifth row onwards, mean wind loads remain constant. This means that the mean wind load coefficients measured at fifth row could represent typical design loads equally applicable to the interior trough collectors in the field. The most important results are summarized in Table 6 [46]. This table lists the critical load configurations for exterior collectors with and without wind fences and interior collectors with and without torque tube. The results shown in Table 6 are a comprehensive design load estimation of trough collectors in array fields at operational and stow modes [46].

To minimize wind loads on trough collectors and optimize wind load distribution over the entire collector field, about 8000 load configurations were analyzed in wind tunnel tests [51,52]. The most important result was the application of photo-bioreactor, which can be regarded as a wind protection device, in the direction of the approaching wind, to reduce wind load actions. The photo-bioreactor is thought to be an effective and economic method that enables experts to minimize and optimize wind loads. Compared to wind loads on conventional, unprotected collectors, the wind loads of collectors with the protection of the photo-bioreactor are much lower in the entire collector field. Whit this protection, maximum loads and moments can be reduced, in average, by more than 70% and more than 50%, respectively, for the overall collector operation range [51].

6. Effects of aspect ratio and porosity and mirror gap on wind loads

Some structural measures to reduce wind loads on solar collectors, including adopting aspect-ratio and porous-edge mirror panels with mirror gaps, were studied in wind tunnel tests. Scientists still have to determine if these measures can reduce wind loads. First, square mirror panels have been universally used by solar collectors and the equilibrium of their wind force components is one of the most important reasons for this. Considering the mechanism of wind flow around collectors, high aspect-ratio mirror panels have their own favorable characteristics, such as relatively low base overturning moment coefficients [47]. Second, porosity and gaps of mirror panels may lead to a

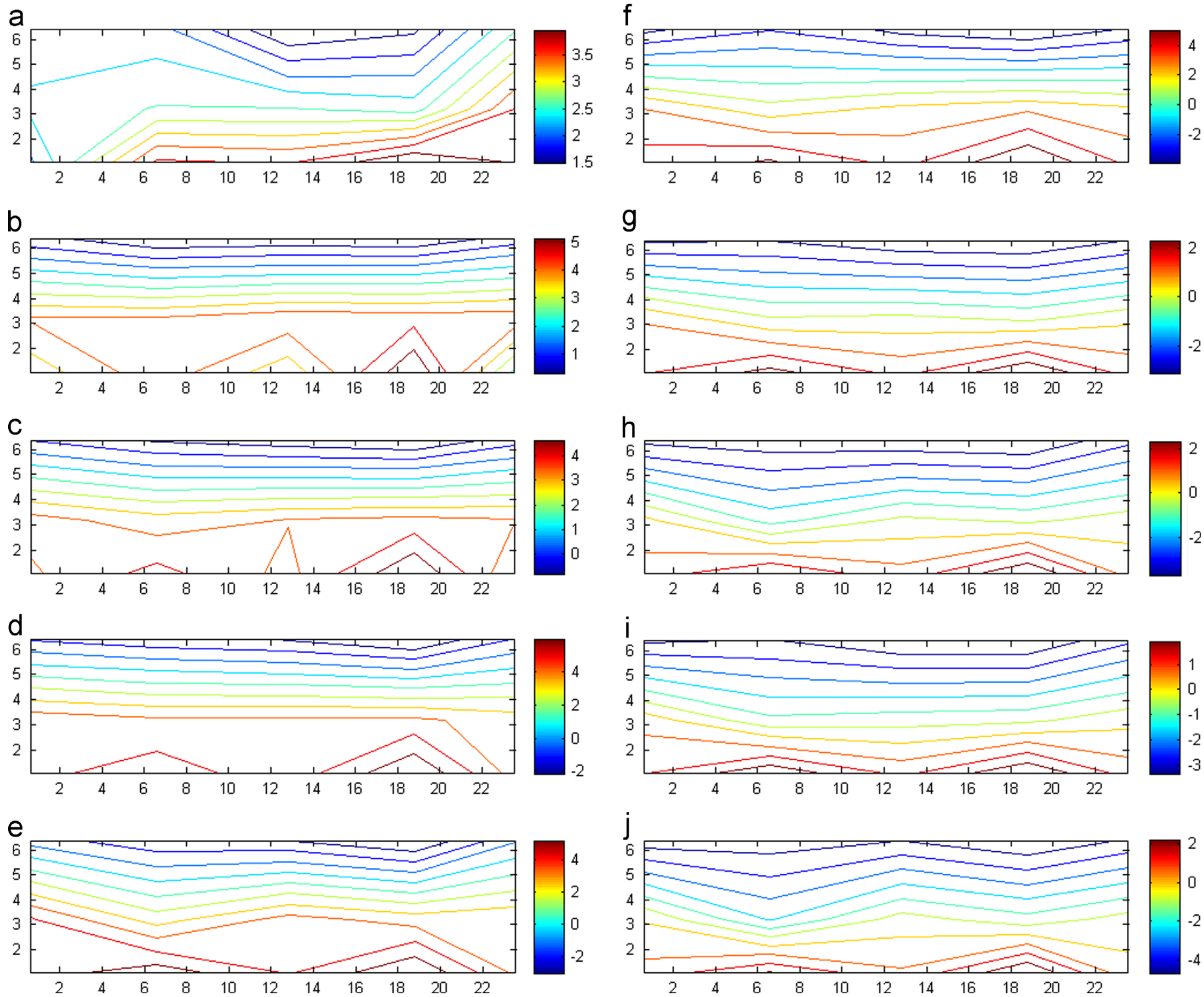


Fig. 8. Net mean wind pressure coefficient contours of trough collector [22]. (a) Pitch = 45 degrees, (b) Pitch = 60 degrees, (c) Pitch = 75 degrees, (d) Pitch = 90 degrees, (e) Pitch = 105 degrees, (f) Pitch = 120 degrees, (g) Pitch = 150 degrees, (h) Pitch = 165 degrees on 8 March, (i) Pitch = 165 degrees on 9 March and (j) Pitch = 180 degrees.

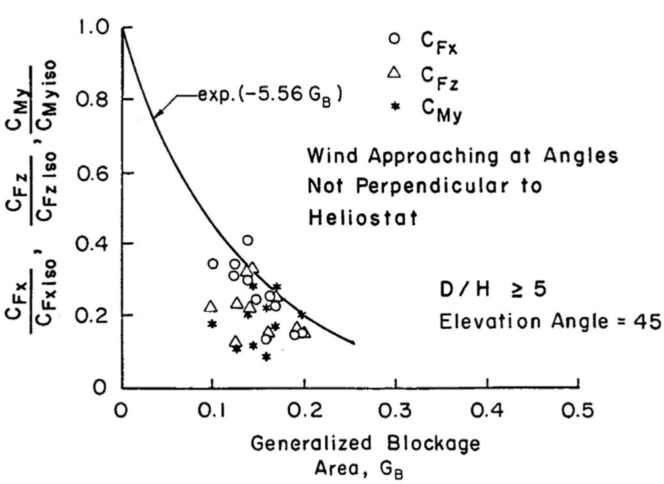


Fig. 9. Mean wind load reduction as a function of generalized blockage [17,18]. D=distance from the heliostat under consideration to external fence, H=height of heliostat at vertical stow position.

different wind flow around solar collectors because of air leaking effects. Air leaking can affect collectors in three different ways, including increasing and decreasing wind loads, or producing a negligible impact on wind loads. These issues are reviewed here to better explain wind load reduction measures and the corresponding wind flow mechanism.

Table 5
Wind load reductions (relative to an isolated heliostat) for high and for low field density [41].

Mode	Operational modes		Stowed mode	
Wind load component\field density	Low (%)	High (%)	Low (%)	High (%)
F_x	30	50	50	60
F_z	10	50	−30	20
M_{Hy}	0	20	20	60
M_y	20	40	40	50
M_z	10	50	None	None

6.1. *Effects of aspect ratio on wind loads of heliostats*

From the point of view of aerodynamics, to select the aspect ratio of mirror panels we need to consider the total wind force components of heliostats. For example, low width–height ratio

Table 6
Critical load cases and load combinations for different groups of the trough collector tests [46].

Case	Condition	Conf.	Yaw	Pitch	CFx	CFz	CMy
(a) Exterior collectors							
Operational mode (positive pitch angles)							
1	Max CFx	B3	30	0	5.097	−0.034	none
2	Min CFx	B4	0	0	−1.242	−0.125	none
3	Max CFz	B3	30	135	2.527	1.849	none
4	Min CFz	B3	0	60	2.107	−5.256	none
5	Max CMy	None	None	None	None	None	None
6	Min CMy	None	None	None	None	None	None
Stow mode (negative pitch angles)							
1	Max CFx	B3	45	−15	5.117	1.550	0.114
2	Min CFx	B4	0	−15	−1.13	−0.404	−0.065
3	Max CFz	B3	0	−60	1.647	3.952	0.364
4	Min CFz	B4	30	−150	2.306	−0.927	−0.232
5	Max CMy	B3	0	−60	1.410	3.709	0.419
6	Min CMy	B3	0	−105	0.870	−0.231	−0.517
(b) Exterior collectors with wind fences							
Pperational mode (positive pitch angles)							
1	Max CFx	D3	45	15	2.900	−0.374	none
2	Min CFx	D3	30	60	−0.503	−0.264	none
3	Max CFz	D3	45	135	1.705	1.030	none
4	Min CFz	D3	45	60	1.175	−2.281	none
5	Max CMy	None	None	None	None	None	None
6	Min CMy	None	None	None	None	None	None
Stow mode (negative pitch angles)							
1	Max CFx	D4	30	−15	4.033	1.026	−0.035
2	Min CFx	D4	−30	−15	−0.852	−0.278	−0.032
3	Max CFz	D5	30	−60	1.294	2.984	0.246
4	Min CFz	D4	30	−135	1.481	−1.050	−0.202
5	Max CMy	D5	30	−45	1.573	2.282	0.332
6	Min CMy	D5	30	−105	0.849	−0.436	−0.468
(c) Interior collectors without torque tube							
Operational mode (positive pitch angles)							
1	Max CFx	C5	30	15	2.264	−0.429	0.113
2	Min CFx	C1	0	0	−1.330	−0.148	−0.098
3	Max CFz	C1	0	120	1.433	1.362	0.370
4	Min CFz	C1	0	75	0.712	−2.533	0.021
5	Max CMy	C1	0	120	1.384	1.081	0.436
6	Min CMy	C1	0	0	−1.228	−0.236	−0.156
Stow mode (negative pitch angles)							
1	Max CFx	C7	0	−30	2.569	1.717	0.134
2	Min CFx	C1	30	−15	−1.374	−0.329	0.025
3	Max CFz	C5	0	−60	1.404	2.754	0.107
4	Min CFz	C5	30	−135	0.859	−0.763	−0.045
5	Max CMy	C5	30	−45	1.929	2.618	0.322
6	Min CMy	C5	0	−90	0.571	0.303	−0.378
(d) Interior collectors with torque tube							
Operational mode (positive pitch angles)							
1	Max CFx	F3	30	0	2.646	0.007	0.005
2	Min CFx	F3	0	0	−1.195	−0.081	−0.053
3	Max CFz	F3	0	105	1.108	1.428	0.463
4	Min CFz	F3	30	60	1.148	−2.155	−0.055
5	Max CMy	F3	30	105	1.139	1.127	0.535
6	Min CMy	F3	30	0	0.157	−0.307	−0.203
Stow mode (negative pitch angles)							
1	Max CFx	F3	30	−15	2.777	0.823	0.051
2	Min CFx	F3	0	−15	−1.475	−0.554	−0.102
3	Max CFz	F3	30	−60	1.478	2.760	0.066
4	Min CFz	F3	0	−90	0.783	−1.127	−0.518
5	Max CMy	F3	30	−30	1.477	1.402	0.315
6	Min CMy	F3	0	−90	0.950	−0.806	−0.629

B3, B4 = collector at edge of field.
C1, C5, C7 = collector at interior of field.
D3, D4, D5 = collector at edge of field with protective fence.
F3 = collector at interior of field with torque tube.

means larger base overturning moment and smaller azimuth moment than for a width–height ratio around 1.0. Likewise, high width–height ratio means smaller base overturning moment and larger azimuth moment than for width–height ratio around 1.0.

Sakamoto and Arie [53] found that the aspect ratio of mirror panels can have a significant influence on the wind loads of heliostats. Pfahl et al. [47] conducted detailed experimental analysis in wind tunnels for selecting suitable aspect ratio.

Table 7
Impact of aspect ratio on wind load components [47].

Load case	α	β	Wind force	Impact r_a	Wind moment	Impact r_a
1	90°	0°	F_x	$1/r_a^{0.35}$	M_y	$1/r_a^{0.85}$
2	30°	0°	F_x	$1/r_a^{0.25}$	M_{Hy}	$1/r_a^{0.65}$
2	30°	0°	F_z	$1/r_a^{0.25}$		
3	90°	60°			M_z	$r_a^{0.35}$
4	0°	0°	F_x	$r_a^{0.45}$	M_{Hy}	$1/r_a^{0.45}$
4	0°	0°	F_z	$r_a^{0.35}$	M_y	$1/r_a^{0.45}$
5	0°	90°	F_y	$1/r_a^{0.25}$	M_x	$1/r_a^{0.15}$

Six heliostat models with the geometric scale of 1:20 were used to measure force components using force balance. Their width–height ratios were 0.5, 1.0, 1.2, 1.5, 2.0 and 3.0. The aspect-ratio effects on wind load components are given in Table 7 [47]. Table 7 shows that the wind force components vary significantly with the variation of the aspect ratios of panels. In most cases, horizontal force, base overturning moment, hinge moment and azimuth moment are important and major force components for the determination of the section dimensions of structural components. For this reason, high width–height ratio is also a reasonable selection for mirror panels. High width–height ratio of panels would lead to the reduction of horizontal force, base overturning moment and hinge moment. However, it also causes the increment of azimuth moment [47].

6.2. Effects of porosity and mirror gap on wind loads of heliostats

Porosity on panels and gaps among panels evidence that air leaking through solar collectors was achieved. In some cases, these measures may change the wind flow around collectors and reduce the wind loads on collectors.

Porous-edge heliostats were measured in wind tunnel tests to determine the porosity effects of wind loads on heliostats [18]. The circular holes were arranged at the perimeter of the mirror panels and the porosity ratio was 35%. The comparative results show that the peak wind loads on the porous-edge heliostat are as large as or larger than those of a solid heliostat without porosity located on the same mirror panel areas. Therefore, porosity on panels is an air leaking measure for the reduction of wind loads on heliostats [18]. Of course, various porosity ratios also need to be investigated to verify the conclusion.

The effects of small gaps between panels on wind loads on heliostats were investigated using the methods of wind-tunnel test and numerical analysis combined [21]. A variation of gap size is from 0 to 40 mm was used. The results show that the small gaps have negligible effects on force component coefficients and wind pressure distribution [21].

Heliostat models with wide gaps between panels were tested in wind tunnels to better understand the gap effects on wind loads on heliostats [41]. Two separated mirror panels constituted the entire reflector of the heliostat. The gap size was 0.5 m wide and the opening ratio was 8%. The comparative results show that the hinge moment coefficients are about 20% higher than those of a heliostat without mirror gaps. And the wide gaps have negligible effects on other force component coefficients. Therefore, wide gaps between panels are not an effective measure to reduce wind loads on heliostats [41].

6.3. Effects of mirror gaps on wind loads on trough collectors

Mirror gaps are thought to be an invalid measure to reduce wind loads on heliostats. It should be investigated if a similar phenomenon occurs on trough collectors.

Two trough collector models with conventional minimum gaps and with enlarged staggered mirror gaps were measured in a wind tunnel [52]. Conventional minimum gap parabola shapes have no aerodynamic effect, compared to completely closed parabolas. The results found that the enlarged staggered gaps have major effects on wind loads of trough collectors. The optimized staggered gap size of 200 mm was deduced by wind tunnel tests. The wind load factors of trough collectors can be reduced by 30% with the staggered gaps between the inner and outer mirror panels [52].

The effects of staggered gaps on wind flow around a trough collector are shown in Fig. 10 by means of Computational Fluid Dynamics simulations [54]. The discrepancies of the gap effects on wind loads of heliostats and trough collectors can probably be classified into two categories. One in which there are differences in collector shapes. Heliostats and trough collectors have an almost flat shape and a parabolic shape respectively, which leads to different wind flows around them. Parabolic shape is beneficial for catching the wind and increasing gaps between the parabolic panels. This can play a part in the variation of wind loads on them. The second category can be described as staggered gap effects. Compared to coplanar gaps, staggered gaps can greatly affect surrounding wind flow. They may also be the cause of vortex formation.

7. Effects of wind on beam quality

The heliostats and trough collectors of solar power stations are located at open fields or suburban areas and they are sensitive to gusts. The deformations wind causes on them will deviate reflected sunlight away from the solar receiver. Therefore, the effects of wind on the beam quality should be a priority in the design of heliostats and trough collectors.

The Beam Characterization System (BCS) is thought to be a reliable tool for evaluating the optical performance characteristics of solar collectors with and without wind action. However, there are some shortcomings for the BCS usage. The actual causes of beam deflection include the twist or bend of the pedestal and the deflection of the supporting structures and mirror panels, which cannot be determined through BCS measurements of the beam movement alone [32]. In addition, the numerical structure analysis can also calculate the beam quality of heliostats and trough collectors under wind action. The expected optical performance of the collectors can be derived from the wind-induced deformations [50].

7.1. Effects of wind on heliostats beam quality

A monitoring program in place from 1986 to 1992 focused on the issues of heliostat beam quality, mirror module performance and durability, tracking accuracy, dynamic wind effects, etc. [32]. The BCS was used to observe and capture successive images of the heliostat beam on the BCS target, while simultaneously recording wind speed and direction data.

Because of local meteorological conditions, the measurements of wind effects on beam quality were performed in a fairly narrow yaw angle range. The ATS heliostat and the SPECO heliostat were tested for comparison purposes. A summary of the measurements are provided in Table 8 [32]. They illustrate the similarity of the optical performance of the two heliostats. For both large-area heliostats, the observed beam deflections under wind action from 12 to 27 mph remain within the specifications for the second-generation heliostat design [32]. The average beam centric movement is 0.9 mrad and the average maximum movement is 1.9 mrad [32].

7.2. Effects of wind on beam quality of trough collectors

Using the numerical structure analysis method, the optical performances of the LS-3 and EuroTrough collectors were analyzed and calculated [50]. First, detailed wind tunnel tests were conducted to get reliable wind loading data. Then, wind-induced deformations were obtained for all members of the collectors by using finite element method calculations. Finally, the expected optical performances of the collectors were derived from these wind-induced deformation results.

The structural twist effects on beam spill were calculated for the three trough collectors, as shown in Fig. 11 [50]. Trough collectors include many mirror modules for a total length of approximately 100 m or 150 m. Wind pressure distribution on the collectors result in larger torque and twist on the supporting tube or truss. Wind speed and structural twist have a major effect on the beam spill. At a wind speed of 11 m/s (25 mph) for operational modes [34], the average structural twist and beam spill would be 8 mrad and 55% respectively [50], which can be referenced for the mechanical and optical analysis of similar trough collectors.

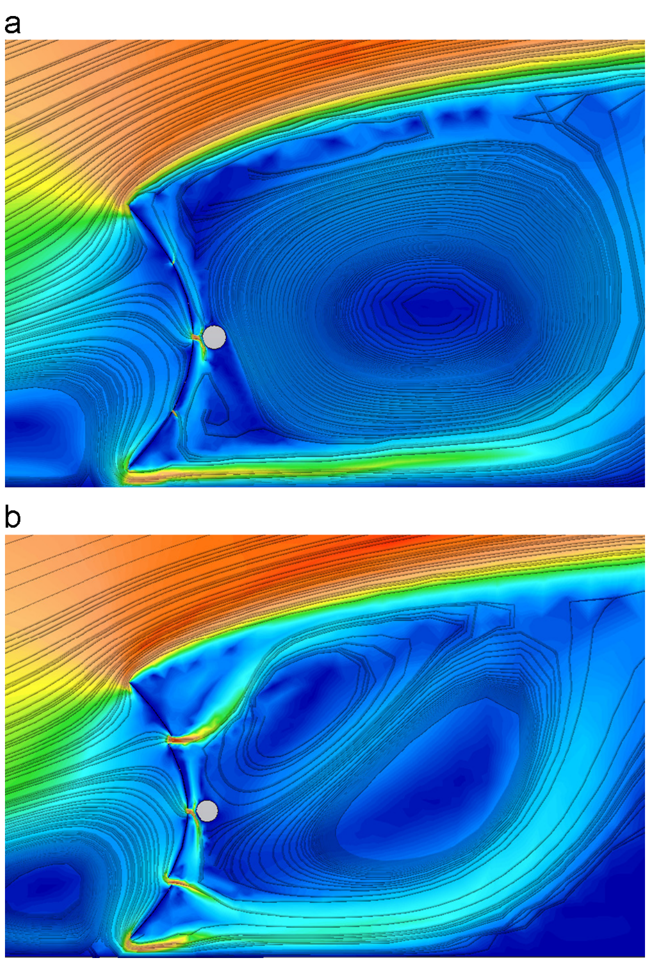


Fig. 10. (a) The effects of coplanar gaps on wind flow around a trough collector by CFD [54] and (b) The effects of staggered gaps on wind flow around a trough collector by CFD [54].

8. Conclusions

The objective of this investigation was to review wind loads on heliostats and trough collectors. The following are some significant conclusions for the evaluation and reduction of wind loads:

(1) Knowing the characteristics of the wind is very useful to understand wind flows around solar collectors. Wind speed profile, turbulence characteristics and wind speed requirements of solar collectors were reviewed here. The wind speed profile with log law has been thought to meet the lowest boundary conditions below 100 m and it is suitable for low structures, such as solar collectors [24,27–29]. Based on considerations of safety and economy, the various CSP technologies have different wind speed requirements [32–34]. The similarity in energy and power spectral densities of approaching wind flow from empirical observations and wind tunnel data would lead to more realistic results of peak wind loads on solar collectors for model scales between 1:10 and 1:40 [41].

(2) Solar collectors are in the highly turbulent field. The variation of turbulence would influence fluctuating wind pressures on heliostats significantly. The conclusion is that wind load coefficients of heliostats increase dramatically for turbulence intensities above 10% [20]. The circular torque tube of heliostats and parabolic mirror edges of trough collectors might be a source of such Re-dependent wind load coefficients. The results show that the wind load coefficients of heliostats and trough collectors are essentially independent of the Re for the range tested [43,46].

(3) Wind loads on an isolated collector can be regarded as baseline for characterizing mechanical and optical performances. There are some discrepancies in the wind force coefficients of heliostats among various wind tunnel tests [20,21,47], which can probably be classified into the effects of experimental models and wide gaps. The wind force coefficients of trough collectors from wind tunnel experiments and field measurements were compared [22,46]. Their variation trends are consistent and the values are a little different between each other. Wind pressure distribution of heliostats and trough collectors were obtained for typical load configurations [22,48]. The distribution can indicate the mechanism of the wind flow behavior around them.

(4) Wind loads on solar collectors laid out in fields are influenced by surrounding collectors and wind fences. The increases of wind fences and field density are effective measures to increase upwind blockage areas, which can reduce wind loads on total heliostats in a field [17,18]. However, in some cases, vertical forces of interior heliostats at stow position increase [41], possibly due to flow separation and vortex shedding

Table 8
Summary of wind effects on beam quality of heliostats [32].

	ATS heliostat	SPECO heliostat
Number of recorded events	11	10
Range of wind speeds	11–27 mph	12–26 mph
Range of yaw angles	92–111°	104–150°
Maximum observed beam deviation	3.7 mrad (at 20.7 mph and 92°)	4.7 mrad (at 17.7 mph and 150°)
Average deviation of beam centroid deviation for all observations	0.92 mrad	0.86 mrad
Average maximum beam centroid deviation for all observations	1.9 mrad	1.9 mrad

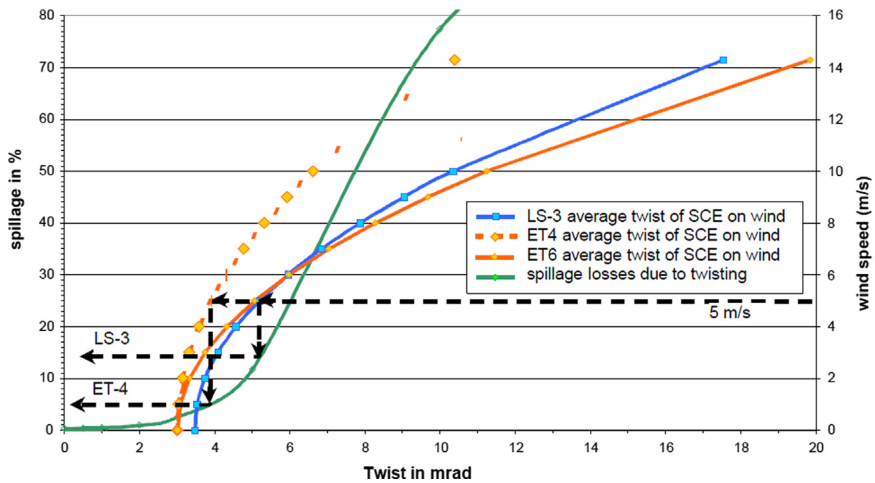


Fig. 11. The wind speed and the structural twist effects on beam spillage for EuroTrough collectors with 100 and 150 m (ET4, ET6) and the reference collector (LS-3) [50].

effects induced by upwind heliostats. For trough collectors, mean wind loads decrease continually from first to fifth row in the approaching wind direction. At the fifth row, mean wind loads reach their minimum values, regardless of the pitch angle. This conclusion is very useful for steel usage design for trough collector at different wind loading zones [46,50].

(5) Wind force components vary significantly with the variation of the aspect ratios of panels of heliostats. Besides square panels, high width–height ratio is also a reasonable choice for mirror panels of heliostats, since high width–height ratio of panels leads to the reduction of horizontal force, base overturning moment and hinge moment. However, it also causes the increment of azimuth moment [47]. Porosity on panels and gaps between panels are thought to be invalid measures to reduce wind loads on heliostats [18,21,41]. The enlarged staggered gaps between the inner and outer mirror panels of trough collector are thought to have major effects on wind load reduction [52], which can greatly affect surrounding wind flow around the collector [54].

(6) The wind-induced deformations of heliostats and trough collectors deviates the reflected sunlight away from the solar receiver. Therefore, the effects of the wind on beam quality should be a priority in the design of heliostats and trough collectors. For ATS heliostats and SPECO heliostats, under wind action from 12 to 27 mph, the observed average beam centric movement is 0.9 mrad and the average maximum movement is 1.9 mrad [32]. For LS-3 and EuroTrough collectors, the wind speed and structural twist have a major effect on the beam spill. At design wind speed of 11 m/s (25 mph) for operational modes[34], the average structural twist and beam spill would be 8 mrad and 55% respectively [50].

Acknowledgments

The work described in this paper was supported by a Research Grant from the Key Laboratory of Solar Thermal Energy and Photovoltaic System, China (National Natural Science Foundation of China, Project no. 51308524), National Basic Research Program of China (2010CB227106) and Beijing Science and Technology Foundation (Z131109000113052)). Finally, the authors are thankful to the reviewers for their helpful comments and suggestions.

References

[1] Solangi KH, Islam MR, Saidura R, Rahimb NA, Fayaz H. A review on global solar energy policy. Renew Sustain Energy Rev 2011;15:2149–63.

[2] Behar O, Khellaf A, Mohammedi K. A review of studies on central receiver solar thermal power plants. Renew Sustain Energy Rev 2013;23:12–39.

[3] Devabhaktuni V, Alam M, Reddy DS, Green RC, Nims D, Near C. Solar energy: trends and enabling technologies. Renew Sustain Energy Rev 2013;19:555–64.

[4] International Renewable Energy Agency. Renewable energy technologies: cost analysis series, volume 1: power sector. Khalidiyah; 2012.

[5] Moser M, Trieb F, Fichter, T. CSP, PV and wind: which technology is the most competitive. In: Proceedings of the 18th international solar PACES symposium. Perpignan, Morocco, Marrakech; 2012.

[6] Coventry J, Pye J. Heliostat cost reduction—where to now. In: Proceedings of the 19th international solar PACES symposium. Perpignan, Las Vegas; 2013.

[7] Denholm P, Mehos M. Enabling greater penetration of solar power via the use of CSP with thermal energy storage. NREL; 2011.

[8] Badescu V, Gueymard CA, Cheval S, Oprea C, Baciu M, Dumitrescu A, et al. Computing global and diffuse solar hourly irradiation on clear sky. Review and testing of 54 models. Renew Sustain Energy Rev 2012;16:1636–56.

[9] Jamel MS, AbdRahman A, Shamsuddin AH. Advances in the integration of solar thermal energy with conventional and non-conventional power plants. Renew Sustain Energy Rev 2013;20:71–81.

[10] Zhang HL, Baeyens J, Degreve J, Caceres G. Concentrated solar power plants: review and design methodology. Renew Sustain Energy Rev 2013;22:466–81.

[11] Fernandez GA, Zerza E, Valenzuela L, Perez M. Parabolic-trough solar collectors and their applications. Renew Sustain Energy Rev 2010;14:1695–721.

[12] Gong B, Li ZN, Wang ZF. Wind-induced dynamic response of heliostat. Renew Energy 2012;38:206–13.

[13] Cermak JE, Peterka JA. Heliostat field-array wind tunnel test. Technical Report for McDonnell Douglas Astrorlautics Company. Report No. CER78-79JEC-JAP-AK2; 1978.

[14] Ewald RL, Peterka JA, Cermak JE. Heliostat-array wind tunnel study. Technical Report for Martin Marietta Aerospace. Report No. CER78-79RLE-JAP-JEC31; 1979.

[15] Randall DE, Mcbride DD, Tate RE. Steady-state wind loading on parabolic trough solar collectors. Technical Report for Sandia Laboratories. Report No. SAND 79-2134; 1980.

[16] Peterka JA, Sinou JM, Cermak JE. Mean wind forces on parabolic trough solar collectors. Technical Report for Sandia Laboratories. Report No. SAND 80-7023; 1980.

[17] Peterka JA, Hosoya N, Bienkiewicz B, Cermak JE. Wind load reduction for heliostats. Technical Report for Colorado State University. Report No. SERI/STR-253-2859; 1986.

[18] Peterka JA, Tan L, Bienkiewcz B, Cermak JE. Mean and peak wind load reduction on heliostats. Technical Report for Colorado State University. Report No. SERI/STR-253-3212; 1987.

[19] Peterka JA, Tan L. Wind loads on heliostats and parabolic dish collectors. Technical Report for Colorado State University. Report No. SERI/STR-253-3431; 1988.

[20] Peterka JA, Derickson RG. Wind load design methods for ground based heliostats and parabolic dish collectors. Technical Report for Sandia Laboratories. Report No. SAND92-7009; 1992.

[21] Wu ZY, Gong B, Wang ZF. An experimental and numerical study of the gap effect on wind load on heliostat. Renew Energy 2009;35(4):797–806.

[22] Gong B, Wang ZF, Li ZN. Field measurements of boundary layer wind characteristics and wind loads of a parabolic trough solar collector. Sol Energy 2012;86:1880–98.

[23] Davenport AG. Rationale for determining design wind velocities. J Struct Eng, ASCE 196039–68.

[24] Simiu E, Scanlan RH. Wind effects on structures—fundamentals and applications to design. New York: John Wiley & Sons; 1996; 42–3.

[25] Deaves DM. Computations of wind flow over changes in surface roughness. J Wind Eng Ind Aerodyn 1981;7:65–94.

[26] Deaves DM. Terrain dependence of longitudinal R.M.S. velocities in the natural atmosphere. J Wind Eng Ind Aerodyn 1981;8:259–74.
[27] Cook NJ. The Deaves and Harris ABL model applied to heterogeneous terrain. J Wind Eng Ind Aerodyn 1997;66:197–214.
[28] Thuillier RH, Lappe VO. Wind and temperature profile characteristics from observations on a 1400 ft tower. J Appl Meteorol 1964;3:299–306.
[29] Tieleman HW. Strong wind observations in the atmospheric surface layer. J Wind Eng Ind Aerodyn 2008;96:41–77.
[30] Li QS, Zhi LH, Hu F. Field monitoring of boundary layer wind characteristics in urban area. Wind Struct 2009;12:553–74.
[31] Prototype/second generation heliostat evaluation and recommendations. Executive Summary for Sandia Laboratories; 1978.
[32] Strachan JW. Testing and evaluation of large-area heliostats for solar thermal applications. Technical Report for Sandia Laboratories. Report No. SAND92-1381; 1993.
[33] Mavis CL. A description and assessment of heliostat technology. Technical Report for Sandia Laboratories. Report No. SAND87-8025; 1987.
[34] Murphy LM. Wind loading on tracking and field mounted solar collectors. Technical Report for Colorado State University. Report No. SERI/TP-632-958; 1980.
[35] Solari G, Piccardo G. Probabilistic 3-D turbulence modeling for gust buffeting of structures. Probab Eng Mech 2001;16:73–86.
[36] Shiau BS, Chen BY. Observation on wind turbulence characteristics and velocity spectra near the ground at the coastal region. J Wind Eng Ind Aerodyn 2002;90:1671–81.
[37] AIJ-RLB-1996. Recommendations for loads on buildings. Architecture Institute of Japan; 1996.
[38] Davenport AG. The spectrum of horizontal gustiness near the ground in high winds. Q J R Meteorol Soc 1961;87:194–211.
[39] Karman T. Progress in the statistical theory of turbulence. Proc Natl Acad Sci 1948;34:530–9.
[40] Banks D. Measuring peak wind loads on solar power assemblies. In: Proceedings of the 13th international conference on wind engineering. Netherlands, Amsterdam; 2011.
[41] Pfahl A, Buselmeier M. Determination of wind loads on heliostats. In: Proceedings of the 17th international solar PACES symposium. Perpignan, Granada; 2011.
[42] Scruton C. An introduction to wind effects on structures. New York: Oxford University Press; 1981.
[43] Pfahl A, Uhlemann H. Wind loads on heliostats and photovoltaic trackers at various Reynolds numbers. J Wind Eng Ind Aerodyn 2011;99:964–8.
[44] ASCE. Wind forces on structures. Trans Am Soc Civ Eng 1961;126:1124.
[45] Peglow SG. Wind-tunnel study of a full-scale heliostat. Technical Report for Sandia Laboratories. Report No. DOE Contract 0E-AC04-760PO0789; 1979.
[46] Hosoya N, Peterka JA. Wind tunnel tests of parabolic trough solar collectors. Subcontract Report for National Renewable Energy Laboratory. Report No. NREL/SR-550–32282; 2008.
[47] Pfahl A, Buselmeier M, Zaschke M. Wind loads on heliostats and photovoltaic trackers of various aspect ratios. Sol Energy 2011;85:2185–201.
[48] Gong B, Wang ZF, Li ZN. Fluctuating wind pressure characteristics of heliostats. Renew Energy 2013;50:307–16.
[49] Wang YG, Li ZN, Gong B, Li QS. Wind pressure and wind-induced vibration of heliostat. Key Eng Mater 2008;400-402:935–40.
[50] Lupfert E, Geyer M, Schiel W, Esteban A, Zarza E, Nava P. Eurotrough design issues and prototype testing at PSA. In: Proceedings of solar forum 2001. Washington, DC; 2001.
[51] Holze C, Brucks A. Optimization of innovative field configurations of parabolic trough collectors and heliostat mirrors by wind tunnel tests. In: Proceedings of the 17th international solar PACES symposium. Perpignan, Spain, Granada; 2011.
[52] Schweitzer A, Schiel W, Ella ZA. Ultimate trough—the next generation collector for parabolic trough power plants. In: Proceedings of the 17th international solar PACES symposium. Perpignan, Spain, Granada; 2011.
[53] Sakamoto H, Arie M. Flow around a normal plate of finite width immersed in a turbulent boundary layer. Trans ASME, J Fluids Eng 1983;105:98–104.
[54] Kotter J, Decker S, Detzler R, Schafer J. Cost reduction of solar fields with Heliotrough collector. In: Proceedings of the 18th international solar PACES symposium. Perpignan, Morocco, Marrakech; 2012.